Astronomy & Astrophysics manuscript no. diffusion
December 21, 2012

Turbulent diffusion of magnetic elements on supergranular scales

F. Giannattasio[1], D. Del Moro[1], F. Berrilli[1], L. Bellot Rubio[2], M. Gosic[2]

[1]Dipartimento di Fisica, Università di Roma "Tor Vergata"
[2]Istituto de Astrofisica de Andalucia
e-mail: Fabio.Giannattasio@roma2.infn.it

ABSTRACT

The study of the spatiotemporal scales on which small magnetic structures are organized, may be approached by determining how magnetic elements are transported by convective motions. The process involved is diffusion. Several works explored the topic, both by simulations and observations. In order to constrain the diffusion process, we analyze the displacement of magnetic elements in time, and the evolution of the mutual distance between magnetic element pairs. We take advantage of Hinode high spatial resolution data of a quiet Sun region at the disk center. The large field of view (∼ 50 Mm) and the long duration of observations (over 25 hours without interruption at a cadence of 90 seconds) allowed us to investigate the turbulent flows at unprecedent high spatial and time scales.

Key words. Sun:

1. Introduction

The dynamics of small scale magnetic structures (magnetic elements) on the solar photosphere is the reflection of turbulent sub-surface convective motions. In the Sun, these flows transport energy from the interior to the surface.
Determining how magnetic elements are transported on the solar surface is crucial to understand on which spatial and time scales the flows are organized. We refer to this topic as the transport problem.

The transport problem is approached in the framework of upper atmosphere heating (e.g. van Ballegooijen et al. 1998). The interaction of magnetic fields with convective flows produces two kinds of disturbances. First, the buffeting of flux tubes by photospheric plasma results in transverse MHD waves (Alfvén 1947), which propagate along the magnetic field and dissipate their energy in the upper layers (e.g. De Pontieu et al. 2007; Tomczyk et al. 2007; van Ballegooijen et al. 2011). Second, the footpoints motion twists and knots the magnetic field lines, creating electric currents in corona that dissipate their energy resistively (Parker 1972, 1983, 1988, 1994; Priest et al. 2002). Both mechanisms are able to heat the corona.
Also, while the flux transport by large-scale flows (such as differential rotation and meridional flows) are easily modeled, the transport by convection cells in the photosphere is still poorly understood (e.g. Berger et al. 1998).

It is demostrated, that three orders of magnitude more magnetic flux emerges in the quiet Sun than emerges in active regions (Thornton & Parnell 2011). In fact, the quiet Sun flux in emerging bipoles is small, but the rate of appearence is large, thus giving the dominant contribution to the solar emerging flux (Martínez González & Bellot Rubio 2009; Ishikawa & Tsuneta 2009). Once emerged, the flux is at first horizontal and settles inside the granules, then appears as a vertical field in the intergranular lanes (e.g. Centeno et al. 2007; Martínez González & Bellot Rubio 2009; de Wijn et al. 2009). Photospheric flows are able to sweep away and avvect the magnetic fields, which then structure in different scales. In a few minutes, the field is avvected from inside the granules to the intergranular lanes (see, e.g., Del Moro 2004, and references therein). On times of hours, the field is avvected in mesogranular scales (5 – 10 Mm, November 1980; November et al. 1981, 1982; Roudier et al. 1998; Roudier & Muller 2004). On times of days, the field is avvected in the supergranular boundaries (20 – 50 Mm, Hart 1956; Simon & Leighton 1964; Berrilli et al. 2003, 2004; De Rosa & Toomre 2004; Del Moro et al. 2004, 2007).
However, there seems to be a continuos spectrum of motions on all scales, from global to sub-granular (see, e.g., Stein & Nordlund 1989; Muller et al. 1992; Shine et al. 2000; De Rosa & Toomre 2004; Roudier et al. 2003; Roudier & Muller 2004).

Despite the efforts, it is still not clear how horizontal velocity fields act on magnetic elements, and how they organize on granular, mesogranular and supergranular scales to produce the observed patches. The turbulent nature of the flows itself is still debeated. The presence of coherent structures and intermittency is in contrast with the standard picture of the turbulent cascade. Nevertheless, most of the turbulent flows present in nature or even in laboratories, are characterized by an ubiquitous presence of coherent structures and internal intermittency (see Petrovay 2001, and references therein for further insights).

Observations at high resolution from Hinode-SOT (Kosugi et al. 2007; Tsuneta et al. 2008) and Sunrise-IMaX (Martínez Pillet et al. 2011) suggest that the generation of the quiet Sun magnetic fields is not fully explainable in terms of decaying active regions (see, e.g., Lites et al. 2008; de Wijn et al. 2009; Lagg et al. 2010; Bonet et al. 2010). Additional mechanisms such as the turbulent dynamo are needed (Petrovay 2001; Pietarila Graham et al. 2010).
In the framework of turbulent dynamo, the fundamental parameter to measure the spreading effect of turbulent flows on magnetic field concentrations is the magnetic diffusivity. This quantity varies with spatial and time scales. The diffusion of magnetic elements on the solar surface follows the law $\langle(\Delta l)^2\rangle \sim \tau^\gamma$, which binds the mean-squared displacements of flows tracers $\langle(\Delta l)^2$ with time τ. When the spectral index γ is unity, the process involved is normal diffusion, and the above equation reads

$\langle(\Delta l)^2\rangle = 4K\tau$, where K is the diffusion coefficient. The case $\gamma \neq 1$ is refered to as *anomalous diffusion*. In this case the quantity $K(\tau) = (\langle(\Delta l)^2\rangle)/4\tau$ is not a constant and scales with a power law $K(\tau) = \tau^{\gamma-1}$ with time. When $\gamma > 1$ the diffusion coefficient increases with scales (super-diffusion); when $\gamma < 1$ the diffusion coefficient decreases when the scales increase (sub-diffusion).

Several works approached the transport problem, and the results are often controversial.
In early numerical simulations Leighton (1964) modeled the diffusion as a random walk, assuming the magnetic elements to be carried passively towards the supergranules boundaries, where they remain until the global field is renewed. He infered that diffusion at the rate of between 770 and 1540 km^{2}s^{-1} is required to reverse the polar field in approximately 10 yr.
On supergranular scales, Mosher (1977) found a flux dispersal consistent with a random walk diffusion with coefficients between 200 and 400 km^{2}s^{-1}, over periods from days to months. To match the Leighton predictions, he supposed the existence of a meridional circulation.
Wang (1988) computed a value of $K \simeq 150$ km^{2}s^{-1} in network regions.
Lawrence & Schrijver (1993) found a sub-diffusive behavior ($\gamma = 0.89 \pm 0.2$) on supergranular scales.
By tracking G-band bright points, Berger et al. (1998) found an increasing diffusion coefficient for increasing time scales (from 50 to 79 km^{2}s^{-1} on time scales from 27 to 40 minutes and from 42 to 57 minutes, respectively).
Hagenaar et al. (1999) found that on short timescales (up to 3 hours), the observed mean-square displacements are consistent with a random walk, characterized by a diffusion coefficient of $70 - 90$ km^2 s^{-1}. On longer timescales (over 8 hours), the diffusion coefficient increases to $200 - 250$ km^2 s^{-1}.
Cadavid et al. (1998) found that in the scale range $16 - 120$ Mm the turbulent part of the flow produces super-diffusive transport.
A year later, Cadavid et al. (1999) found a sub-diffusive transport regime ($\gamma = 0.76 \pm 0.004$) on timescales lesser than 20 minutes, and normal diffusion ($\gamma = 1.10 \pm 0.24$) for times larger than 25 minutes. The sub-diffusion is due to the presence of stagnation points, causing a broad waiting time distribution.
Lawrence et al. (2001) found a superdiffusive behavior with $\gamma \simeq 1.1$, but obtained a Kolmogorov "K41" scaling by computing magnetic bright point velocities. The interpreted these results as due to the imperfect correlation between tracers and the undelying fluid flow. Abramenko et al. (2011), analyzing G-band bright points, found a superdiffusive regime, with a spectral index changing with the observed environment (quiet Sun, coronal hole, plage area), spatial and time scales.
By observing small magnetic structures on very quiet regions Manso Sainz et al. (2011) detected a drift motion superposed to a random walk, on granular scales. Within the integranular lanes they found a pure random walk with a constant diffusion coefficient of 195 km^{2}s^{-1}. A vortical motion may appear at scales $\lesssim 400$ km.

An important issue in the transport problem is the study of pair dispersion of magnetic elements.
While the scaling properties of diffusion of single Lagrangian particles are driven by the large scale eddies, the pair dispersion reflects the diffusivity properties on scales of the order of the separation of the pairs. Thus, the pair dispersion problem reflects the nature of the inertial range of turbulence, independently of the large scale flow, and the intermittency in the energy cascade. The latter manifests in those pairs which remain close each other for long periods (see Biferale et al. 2005, and references therein).

In the work of Berger et al. (1998), mesurements of the relative motion of random pairs of objects were performed. They argued that such an analysis reveals any systematic behavior in the dispersion. They found a separation incresing with time consistently with a diffusion process not strongly non-Gaussian ($\gamma = 1.34 \pm 0.06$).
Rast & Pinton (2011) studied the pair dispersion in turbulent regimes, emphasizing the importance of delay times, the distribution of which has great influence on the pair separation scaling laws. The initial pair separation is also a fundamental parameter: the bigger, the broader is the delay times distribution. They concluded that scaling is not prevented by lack of dynamics into the inertial range, but it is blurred by intermittency, which widens the distribution of delay times.
By utilizing the Lagrangian approach in the framework of turbulent pair dispersion, Lepreti et al. (2012) analized the same observations as in Abramenko et al. (2011). Unlike those authors, they found that $\gamma \simeq 1.5$ has nearly the same value for a plage area, a quiet Sun region and a corona hole region. They attributed this difference to the fact that pair dispersion reflects the diffusivity properties arising from the local correlations in the inertial range of turbulence; on the contrary, single particle diffusion is influenced by the detailed structure of the velocity field.

In this paper we use both the single and pair dispersion approaches in order to measure the diffusion of magnetic elements on supergranular scales. We take advantage of Hinode high spatial resolution and 25 hours uninterrupted observations of a quiet Sun region at the disk center.
The paper is structured as follows. In section 2.1 we describe our data set. In section 2.2 we describe the tracking algorithm for magnetic elements. In section 3.1 we show the lifetime statistics of magnetic elements. Sections 3.2 and 3.2 are devoted to show the results obtained for single and pair dispersion approach, respectively. In section 4 we discuss our findings. In section 5 we draw conclusions.

2. Observations and data analysis

2.1. The Hinode data set

Our data set consists of time series of magnetograms, dopplergrams, and continuum intensities of the same quiet Sun region at the disk center (Figure 1).
The data correspond to the Na I D line at 589.6 nm, observed at two wavelengths (±160 mÅ from the line center) with the Hinode Narrow-Band Imager (Kosugi et al. 2007; Tsuneta et al. 2008). The data are 2×2 binned, corresponding to a pixel area of 0.16×0.16 arcsec^2.
The noise in the magnetograms is 4 Mx cm^{-2} (or 4 G). This was computed as the rms fluctuation of the signal in a region without obvious magnetic fields.
Each series starts at 08:00:42 UT on November 2, 2010. The observations were performed at a cadence of 90 s. The total duration is 25 hour without interruptions (995 frames).
All the data have been subsequently co-aligned, trimmed to the same FOV, and filtered for five-minute oscillations.
The large FOV (about 51×53 Mm^2) allows us to observe a supergranular cell, as clearly visible in Figure 1a. In that Figure the magnetogram has been saturated at ±25 G to emphasize the weak magnetic fields in the quiet Sun.
The long observation allows us to observe the evolution of the supergranular cell, up to its final stages, when only the strong

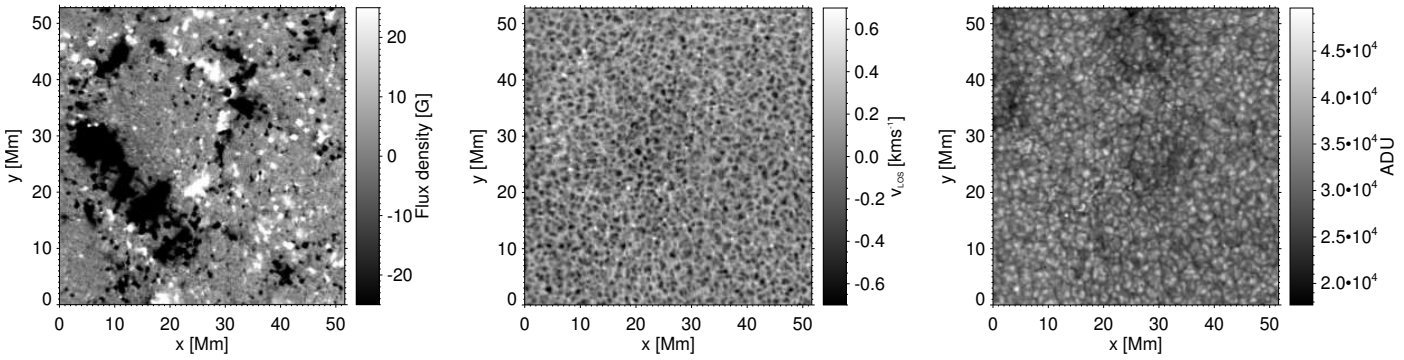

Fig. 1. Hinode magnetogram (a), dopplergram (b) and intensity map of a region in the disk center at 08:00:42 UT, corresponding to the beginning of the time series. To see the evolution of the magnetic flux without flickering images, magnetograms are saturated at ±25Mx cm^{-2} and dopplergrams between ±0.7 kms^{-1}.

magnetic field concentrations remain, and the supergranule tends to dissolve.

2.2. Tracking the magnetic elements

This paragraph explains the detail of the recognition and tracking of the magnetic features.

The first part is the segmentation of the magnetogram image. The segmentation is obtained via an iterative algorithm similar to Del Moro (2004). At every step i, the selection threshold $T_s(i)$ (note that $T_s(0) = 0$) is raised by an amount $\Delta T_s = 3 \cdot \sigma$. All the pixels whose $B(x, y) > T_s(i)$ are flagged as magnetic pixels, the rest is discarded. All the flagged pixels which are clustered in groups smaller than $A_{max} = 50$ *pixels* are recognized as segmented features and labeled. The rest of the flagged pixels (composed of large connected regions) is instead selected for the $i + 1$ iteration with threshold $T_s(i + 1)$. Since segmenting the magnetogram with a single threshold will lead to either the loss of the low B structures or the merging of high B structures in big clusters, we realized this iterative procedure to resolve both the low B structures and the peaks of the larger magnetic features.

The segmented time sequence is therefore used to reconstruct the trajectory of the magnetic features. The tracking algorithm tries to link each labeled feature present at time t with a corresponding labeled feature at time $t+\delta t$. The constrains used are:

- Cospatiality: the feature gravity centres must be closer than 3" in subsequent frames.
- Similarity: the feature shapes cannot be different by more than 150%.
- Exclusivity: once a feature has been linked to a trajectory, it cannot be used for any other trajectory.

If the search for a corresponding feature at time $t + \delta t$ fails, the algorithm extends the research to the $t + 2\delta t$ frame. If also in that case the algorithm finds no suitable feature to be linked to the current feature trajectory, the trajectory ends.
All the features succesfully tracked for more than $\Delta t_{min} = 360$ (4 frames) are included in the tracked structured database used in the following analysis.

According to these criteria, a total of 20145 magnetic elements were tracked. Their lifetime ranges from 7.5 minutes (5 frames) to 11.1 hours (444 frames).

3. Results

3.1. The lifetime of magnetic elements

The mean magnetogram shown in Figure 2 allows us to recognize the "persistent" magnetic fields, which settle mainly on the edges of the supergranule. This is the place were we expect to find the most enduring magnetic elements. In Figure 2, the tracks relative to the 50 longest living magnetic elements are represented.

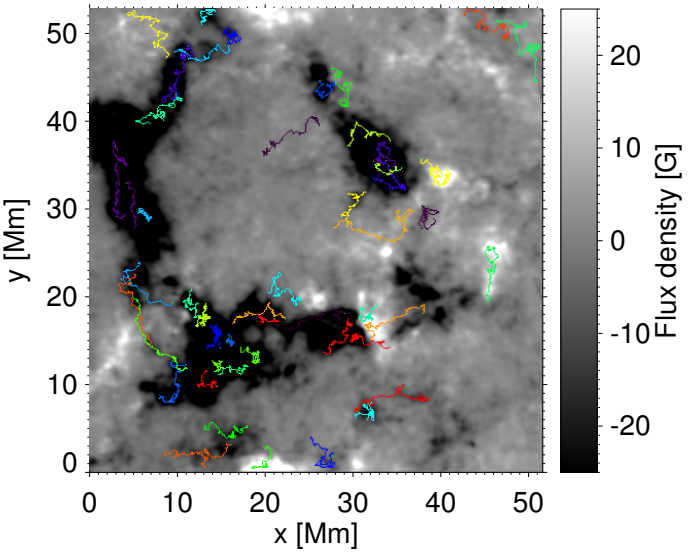

Fig. 2. Mean magnetogram saturated at ±25Mx cm^{-2}. The coloured tracks represent the trajectories of the 50 longest living magnetic elements. Their lifetime spans the range from ∼ 4 to ∼ 11 hours.

By using the standard IDL libraries, we applied an erosion operator to the mean magnetogram. On the resulting segmented image, we traced a polygonal region of interest (ROI) enclosing the supergranule (see Figure 3). We computed its area to be $\simeq 1.336 \cdot 10^3$ Mm^2.
The location of the first appearence has been used to decide

whether each magnetic element belongs to the ROI or not. We selected separately the magnetic elements within the ROI, those outside the ROI, and those on the boundaries of the supergranular cell. We found that the ROI hosts a total of 10123 magnetic elements, 2522 of which lie on the boundaries of the supergranule. The remaining 10022 magnetic elements are outside the ROI.

In Figure 4 we show the magnetic elements lifetime histogram.

The lifetime distributions within the supergranule, out of the supergranule, and within the boundaries, are well fitted by exponential functions up to $\sim$ 2000 s. As the time increases, the statistics drops, and the χ^2 increases. We note that the lifetime distribution of magnetic elements in and out of the supergranule are very similar, apart from slightly different counts. This result is somewhat expected, because the outer supergranule corresponds to the inner of a neighbor supergranule.

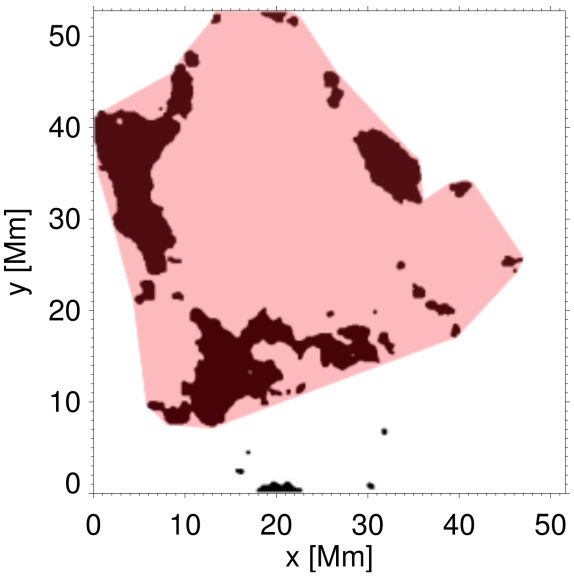

Fig. 3. Segmented output image obtained from the mean magnetogram shown in Figure 2. The shaded area corresponds to the ROI.

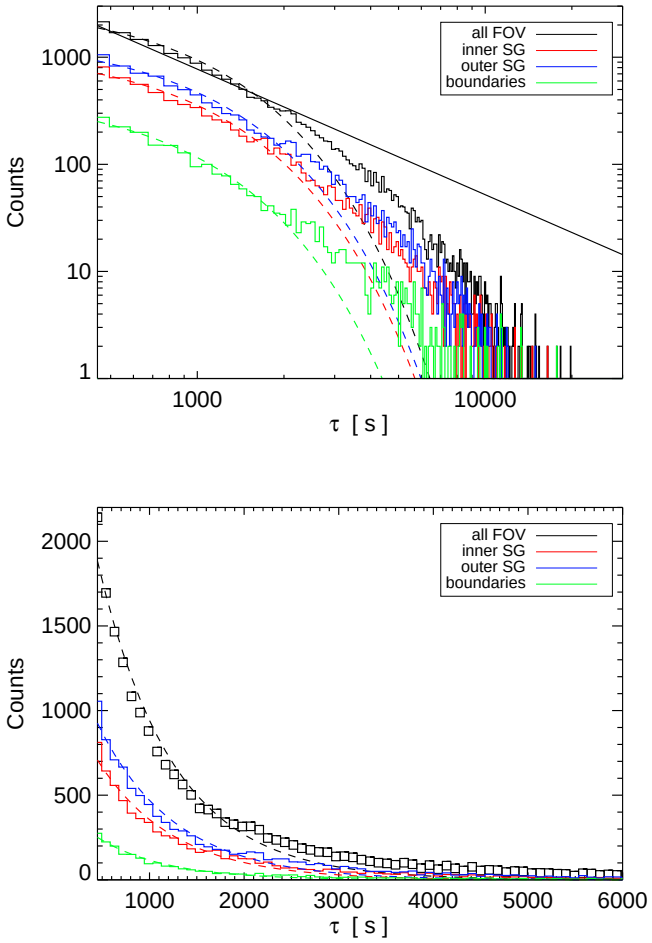

Fig. 4. In the lower panel: lifetimes histogram of the magnetic elements in the FOV (black) and its components: inside the ROI (red), outside the ROI (blue), and within the boundaries of the supergranular cell (green). The time τ is computed respect to the first detection. Dashed curves are exponential fits. The log-log plot in the upper panel allows to see more clearly the behavior on the longest time scales. The black continuos line is a power-law fit to the distribution of lifetimes in all the FOV.

3.2. One-point diffusion

In the framework of diffusion in turbulent fields, it is customary to follow a Lagrangian approach, which is able to describe the statistical properties of particles choosen as tracers of the flows. On the solar photosphere, magnetic elements may have the same role of such tracers, provided that the associated magnetic field strength is weak enough to be regarded as passively transported by the flows.

In Figure 5 we show the magnetic flux distribution as retrieved from the mean magnetogram. The flux is mainly unipolar (negative), peaks at 0 G and drops steeply: the number of structures at -50 G is approximately 1% of those at 0 G. The weakest part of the distribution ($|\mathbf{B}| < 23.5$ G) is dominated by the magnetic fluxes located inside (outside) the ROI. The higher unipolar fluxes are present only in the boundaries of the ROI. Specifically, we find that the boundaries of the supergranule cover $\sim$ 11% of the FOV, and account for $\sim$ 61% of the total magnetic unsigned flux. The weak magnetic fields inside the ROI are spread on $\sim$ 38% of the FOV, and represent $\sim$ 21% of the total magnetic unsigned flux. The remainig percentages are due to the magnetic fluxes outside the ROI, which however belong to an adjoining supergranule.

The volume forces acting on magnetic elements, when considering them as thin flux tubes, are the buoyancy $F_b \sim B^2/2\mu_0 H_P$ and the curvature $F_c \sim B^2/\mu_0 l$, which are of the same order (H_P and l are the pressure scale height and the correlation length, respectively). Also a surface force acts on flux tubes: the drag force $F_d \sim \rho v^2/d$ due to the plasma kinetic energy (d is the diameter of the flux tube, ρ is the plasma density and v the turbulent velocity).

Typical values for plasma density and velocity in photosphere are $\rho \sim 2 \cdot 10^{-7}$ gcm^{-3} and $v \sim 1$ kms^{-1}. The equipartition field B_e, for which $B_e^2/2\mu \sim \rho v^2/2$, is then $B \simeq 160$ G.

The pressure scale height in the solar photosphere may be roughly estimated to be $\sim$ 300 km, after setting $T \simeq 5700$ K and modeling the atmosphere as consisting of only hydrogen.

In the boundaries of the supergranular cell under examination, where the strongest and longest living flux concentrations are observed, the flux is at most $|\mathbf{B}| \sim 250$ G (see Figure 5). For those very few magnetic fields, by assuming diameters of $\sim$ 800

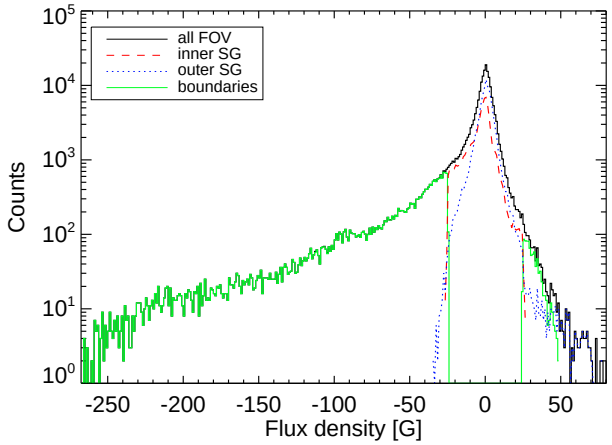

Fig. 5. Magnetic flux distribution as retrieved from the mean magnetogram (black). In red, blue and green the contributions from inside the ROI, outside the ROI and the boundaries of the ROI, respectively. Vertical green lines at −23.5 G and 23.5 G separate the weak from the strong fields at the boundaries of the ROI.

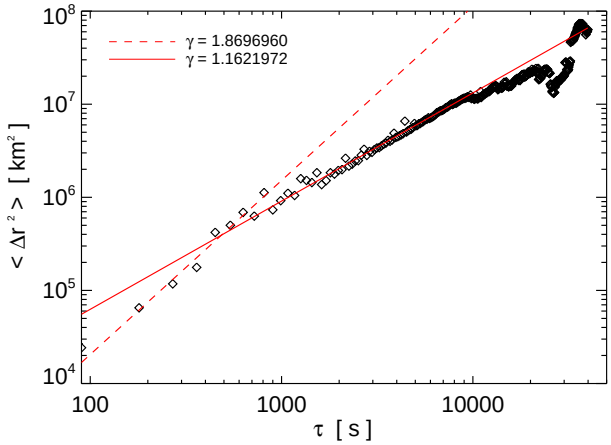

Fig. 6. Displacement spectrum for all the 20145 magnetic elements tracked in the FOV. The dashed line fits the data point up to ∼ 1000 s; the continuos line fits the data points up to ∼ 9000 s.

km (the maximum diameters we tracked), we find $F_d \sim F_b$. This means that for almost all flux tubes we have $F_d \gg F_b \sim F_c$. Thus, we can approximate the field inside the ROI to a passive driven by the supergranular flow.

As pointed out in the introduction to this paper, further insights on the nature of diffusion can be given quantifying the index γ of the displacement spectrum $\Delta r^2(\tau) \sim \tau^\gamma$.
For each magnetic element i we computed the displacement Δr_i as a function of time τ, evaluted since the first appearence. Then, for each time step, we computed the averaged square displacement (hereafter displacement spectrum)

$$\Delta r^2(\tau) = \langle \Delta r_i^2 \rangle_i.$$

In Figure 6 we show the displacement spectrum in time for all the 20145 magnetic elements tracked. Such a spectrum has been fitted with power laws, separating the contributions at lower and higher time scales. We obtained a spectral index $\gamma \sim 1.87$ for time scales up to 1000 s and $\gamma \sim 1.16$ for times scale up to 9000 s. At even higher time scales the number of surviving magnetic elements is too small to reach any conclusion on the spectral index, and features due to the poor statistics appear in the spectrum.

When anomalous diffusion holds, the diffusion coefficient is dependent on both spatial and time scale (Abramenko et al. 2011):

$$K(\Delta r) = \frac{c\gamma}{4}\left(\frac{\Delta r^2}{c}\right)^{\frac{\gamma-1}{\gamma}}$$

$$K(\tau) = \frac{c\gamma}{4}\tau^{\gamma-1}$$

where c, and γ are retrieved by the linear fits in Figure 6.
In Figure 7 we show $K(\Delta r)$ and $K(\tau)$. In both panels, we separated the contribution from the two regimes observed in Figure 6. The diffusion coefficients range from 100 to 700 km^{2}s^{-1}. The super-diffusive behavior is evidenced by the monotonic growth of the diffusion coefficient with the spatial and time scales.

3.3. Pair diffusion

Once established the magnetic elements are passively swept by the photospheric flows, we can approach the transport problem also by means of pair dispersion.
The analysis is the same as in previous section, except that this time $\Delta r^2(\tau)$ assumes the meaning of a pair separation spectrum in time.
The initial ($\tau = \tau_0$) pair separation Δr_0 is an essential parameter, as it sets the spatial scale of the problem (see, e.g. Biferale et al. 2005, and references therein). In principle, it could assume any value between a certain lower limit to the length size of the whole system concerned. In order to estimate the lower limit for Δr_0 we considered the area distribution in time of each magnetic element tracked. Even considering the change in area during the evolution, a maximum value of $A_{max} = 49$ pixels^2 may occurr. It corresponds to a maximum radius of $r_{max} = \sqrt{A_{max}/\pi} \simeq 8$ pixels, when approximating each magnetic element shape to a circle. Thus, the minimum distance between two magnetic elements may be estimated as $d_{min} = 2 \times r_{max} = 16$ pixels, which corresponds to 1856 km on the photosphere, i.e. nearly twice the typical size of granules.

We selected all pairs in the FOV with $d_{min} < r_0 < 43$ pixels (∼ 5 Mm). This request left 163926 pairs. We fitted the separation spectrum to a power law with the following spectral indeces: $\gamma \sim 1.27$ for time scales up to 1000 s, and $\gamma \sim 1.01$ for times scale up to 9000 s. These results are shown in the upper panel of Figure 8.

In order to avoid the strong inhomogeneities of the velocity field in the FOV, we focused on the inner supergranule. We selected a circular region centered in the centroid of the supergranular cell, such that its radius R_s is always lower than the distance between the center and the inner boundary. A total of 68707 pairs were found therein. The initial separation r_0 spans the range $d_{min} < r_0 < 2R_s$.
We obtained the separation spectrum shown in the lower panel of Figure 8. The spectrum is well fitted by a power law with spectral index $\gamma \sim 1.6$.

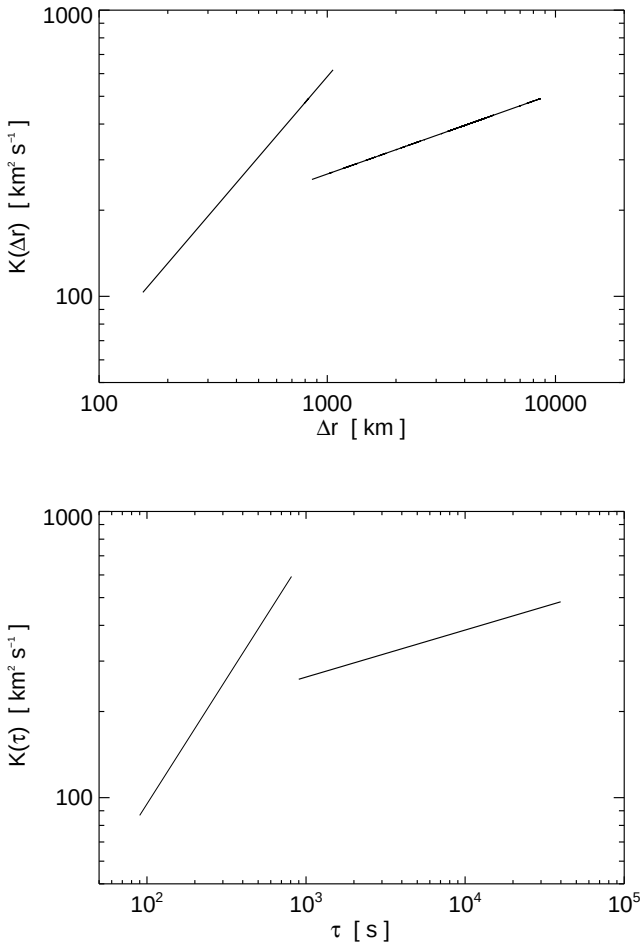

Fig. 7. Upper panel: Diffusion coefficient as a function of the spatial scale. Lower panel: Diffusion coefficient as a function of the time scale. Both scale-dependent coefficients are retrieved by the fits in Figure 6, following the formulas provided in Abramenko et al. (2011).

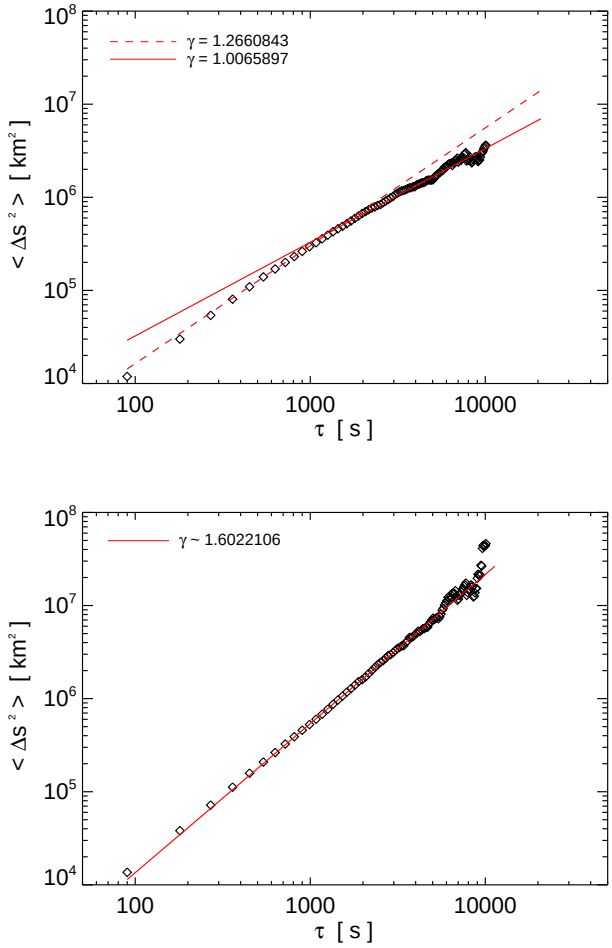

Fig. 8. Upper panel: Pair separation spectrum of the magnetic elements with r_0 up to 5 Mm. The dashed line fits the data point up to ~ 1000 s to a power law with spectral index $\gamma \sim 1.27$. The continuos line fits the data points up to ~ 9000 s to a power law with spectra index $\gamma \sim 1.01$. Lower panel: Pair separation spectrum on supergranular scales. The best fit corresponds to a power law with spectral index ~ 1.6

4. Discussion

In the framework of turbulent diffusion, it is fundamental to investigate the dynamical properties of the photosphere both at high spatial resolution and fast cadence. It is also crucial to avoid the disturbances introduced by the earth atmosphere, which greatly limit the resolutions available and, far worse, introduce spatial and time scales that have nothing to do with the Sun's atmosphere.
HINODE observations permitted us to explore the diffusion properties of 20145 magnetic elements at unprecedently high spatial and time scales, combined with high spatial resolution and seeing-free observations.

In Figure 2 a network magnetic field is clearly visible to outline a supergranule. As expected, the longest living magnetic elements are located in the boundaries of the supergranule, where the strongest magnetic fields are observed (e.g. Liu et al. 1994; Zhang et al. 1998). The stronger the magnetic field, the greater the inertia it opposes to the flow. In such environment, the magnetic field can survive longer to the spreading action of diffusive flows.

The lifetime histogram in Figure 4 shows that the statistics of short living magnetic elements is dominated by the inner and the outer supergranule. Such regions are covered by almost 10 times more magnetic elements than the boundaries.
It is worth nothing that the shape of the distribution for inner and outer supergranular magnetic elements is very similar, apart from slightly different statistics. This is somehow expected, because the outer region corresponds to the inner region of an adjoining supergranule. This makes no sense to distinguish the inner from the outer region.

At higher time scales the statistics is dominated by the boundary regions (as shown also in Figure 2).
We note that as long as the counts number is high (down to ~ 5% of the starting magnetic elements), the histogram is well fitted by an exponential decay. This agrees with the observations of Zhou et al. (2010) for IN magnetic fields. As the counts number drops the distributions broaden, and their shapes are between exponential and power laws.

The distribution of magnetic flux shows a sharp peak at null strength, with a steep decreas up to $|\mathbf{B}| \sim 50$ G, after which only the boundary fields survive. This is an important issue, because enables us to deal with the magnetic field as passively transported by the turbulent photospheric flows. This

assumption is the basis of the analysis performed in this work. Of course, the passive hypothesis is more strictly verified in the inner (outer) supergranule. Nevertheless, we also investigated the diffusion problem in the whole FOV, not explicitly separating the behavior from different supergranular regions. An implicit separation is present, because of the longest living magnetic elements bias toward the supergranule boundaries. In fact, we know that the longest time scales are populated almost only by the boundary magnetic fields. Moreover, introducing region separations drastically reduces the statistics of available magnetic elements into each region.

It is not clear yet how magnetic fields in the quiet Sun are generated. The observations in the space and baloon era (Lites et al. 2008; de Wijn et al. 2009; Lagg et al. 2010; Bonet et al. 2010) seem to rule out the decay of active regions. In this context, the diffusion of magnetic tracers on the photosphere may help to shed light on the mechanisms that generate the local magnetic field concentrations in the quiet Sun.
We investigated these topics at unprecedently high space and time scales (i.e. supergranular), and spatial resolution (0.16 arcsec/pxl). By examining the displacement spectrum, we found a superdiffusive behavior in the whole FOV. This means that the diffusivity, which is a measure of the flow capability to create or destroy magnetic field concentrations, is a scale dependent quantity. This fact is very important, because rules out simple random walk scenarios. In particular, a $\gamma > 1$ value implies a diffusion coefficient increasing with scale. In this case the diffusivity is small enough to allow the small scale aggregation of magnetic elements. Otherwise, a subdiffusive regime ($\gamma < 1$) implies a diffusivity growing on smaller scales. This prevents magnetic field concentrations to withstand the spreading action of velocity fields.
Our findings of a highly super-diffusive regime ($\gamma \sim 1.87$) on time scales $\tau \lesssim 1000$ s (τ_c), are consistent with a turbulent dynamo scenario, in which the co-operation of small scale magnetic fields allows the formation of the magnetic structures that are observed in the quiet Sun. We note that $\gamma \sim 2$ corresponds to a ballistic motion due to one-way advective flows towards the boundaries of supergranules. At larger scales ($\tau > \tau_c$ s), the diffusion regime is much closer to a random walk ($\gamma \sim 1.16$). This may be explained by the combination of two effects.
First; on time scales $\sim \tau_c$ magnetic elements migrate frome the site of emerging to cell boundaries. They are trapped therein and eventually aggregate at velocity field sinks (stagnation points). As the whole supergranule evolves, these sinks displace randomly (Simon et al. 1995).
Second; as magnetic elements approach and settle in granular and/or supergranular boundaries, their "inertia" is increased because of aggregation. This lowers the diffusion rate.

Anomalous diffusion is due to the variation of diffusivity with scales. From a mathematical point of view, as the diffusion coefficient depends on the spectral index, the changing diffusion regime is also manifested in the change of the slopes in Figure 7. At critical space and time scales of $\Delta r_c \sim 1000$ km (~ 1 Mm) and $\tau_c \sim 1000$ s (~ 15 min), respectively, an abrupt change in diffusivity is observed: values drop from ~ 700 to ~ 250 km^{2}s^{-1}. These results may be interpreted in terms of the coupling between magnetic elements and fluid motions (Lawrence et al. 2001). When a significant coupling holds and the correlation time is finite, a superdiffusive behavior is expected. In the case of a brief correlation time, normal Brownian diffusion holds. For times lower than the critical, a ballistic motion is observed due to unidirectional advection of magnetic elements (Cadavid et al. 1999). On critical scales we observe a transition between such a highly superdiffusive regime and a regime much closer to a random walk. As magnetic elements move always along the intergranular lanes, the change of regime may be due to the renewal of velocity field on granular space and time scales. The new field may change the pattern of downflows, resulting in a random motion for magnetic elements.

Since Richardson (1926), the diffusion problem was addressed in the framework of isotropic turbulence by the dispersion of pairs of particles. Unlike the single particle diffusion, which is mostly driven by the large scale eddies, the pairs dispersion depends on fluctuations of the order of separation of pairs, i.e., the quantity

$$\mathbf{r}(\tau) = \mathbf{r_0} + \int_0^\tau \mathbf{w}(\tau')d\tau'$$

where $\mathbf{w}(\tau)$ is the relative velocity between the particles and $\mathbf{r_0}$ the initial separation vector. If both $\mathbf{r_0}$ and $\mathbf{r}(\tau)$ lie in the inertial subrange, then $\langle|\mathbf{r}(\tau) - \mathbf{r_0}|^2\rangle \sim r_0^{2/3}\tau^2$ for $\tau \ll \tau_B$, and $\sim \tau^3$ for $\tau \gg \tau_B$, where τ_B is the time after which dispersion becomes independent of $\mathbf{r_0}$ (Batchelor 1950), namely the eddy turnover time associated to initial separation $\mathbf{r_0}$. These scaling regimes are very difficult to observe for the need of very long inertial subranges.

By applying the pair dispersion approach to our dataset, we retrieved the separation spectrum first considering the whole FOV, then restricting to the inner supergranule (see Figure 8). In the former case we found a slightly superdiffusive regime for $\tau < \tau_c$, and a random walk for $\tau > \tau_c$. In the latter case the scaling changed by an increase of the spectral index. This result was somewhat expected, because of the inhomogeneities of the environment. The double slope is a signature of different regimes at work. In fact, taking the entire FOV corresponds to mix the statistics of very mobile magnetic elements in the center of the cell, and slow boundary elements. This mixing manifests as a γ ranging between 1 (that should be observed in the boundaries) and 1.6 (which is observed in the inner supergranule). What is shown in lower panel of Figure 8 represents our final result on the dispersion of magnetic elements on supergranular scales.

As mentioned before, the single particle and the pair dispersion give different information, and it is not surprising that different regimes (i.e., different γ) are observed. In any case the spectral index is far from a Batchelor or Richardson scaling. This may be due to three reasons: 1) we are in a mixed transient state between the Batchelor and the Richardson regimes. The investigation of spectra for a large number of $\mathbf{r_0}$ enhances the probability of observing the transition between such regimes; 2) the resistence opposed by stronger magnetic fields to the flows must be taken into account. Even in high Reynolds media, more magnetized elements diffuse slower (see,e.g., Schrijver & Martin 1990; Berger et al. 1998; Hagenaar et al. 1999); 3) the problem is not consistent with a turbulent scenario, or at least with homogeneous and isotropic turbulence.

It is important to note that the diffusion coefficient for relative dispersion in isotropic turbulence is not unique. Any scaling $K(\Delta r, \tau) \sim \langle\epsilon\rangle^a \tau^b \Delta r^c$ satisfying $2b + 3c = 4$ and $a = 1 - c/2$ yield $\langle|\mathbf{r}(\tau) - \mathbf{r_0}|^2\rangle \sim \tau^3$ (Klafter et al. 1987). Deeper investigations involving the probability density function $p(r, \tau|r_0, \tau_0)$ are necessary in order to fully understand the process underlying the diffusion of magnetic elements on the photosphere.

5. Conclusions

Determining how magnetic elements are transported on photosphere by convective motions may help to understand on which space and time scales flows are organized, and how much energy magnetic fields can store and eventually transfer to the upper layers. Using unprecedently HINODE data, we analyzed the displacement of magnetic elements in time, and the evolution of mutual distance between magnetic element pairs. The high resolution, the large field of view ($\sim$ 50 Mm), and the very long duration of observations (over 25 hours) allowed us to investigate photospheric flows up to supergranular scales. As expected, the longest living magnetic elements lie on the supergranule boundary, where the highest magnetic fluxes are observed. The displacement spectrum for single magnetic elements shows a double-regime behavior: highly superdiffusive ($\gamma \sim 1.87$) up to granular scales, and slightly diffusive ($\gamma \sim 1.16$) for longer scales up to supergranular. This is probably due to the almost-random evolution of the sites into which the magnetic elements fall on τ_c scales. In both the observed regimes, the scale dependent diffusivity ranges between $\sim$ 700 and $\sim$ 250 km^{2}s^{-1}. However, the breaking scales emerging τ_c and Δr_c are the granular ones. Pair dispersion analysis in the inner supergranule shows a regime intermediate between Batchelor and Richardson scaling ($\gamma \sim 1.6$). This may be due to the stiffness opposed by magnetic elements to dispersion, and to the inapplicability of homogeneous and isotropic turbulence scenario to the real solar photosphere.

Lastly, we note that the only breaking scales emerging in both analysis are the granular ones.

Acknowledgements. *Hinode* is a Japanese mission developed and launched by ISAS/JAXA, collaborating with NAOJ as a domestic partner, NASA and STFC (UK) as international partners. Scientific operation of the Hinode mission is conducted by the Hinode science team organized at ISAS/JAXA. This team mainly consists of scientists from institutes in the partner countries. Support for the post-launch operation is provided by JAXA and NAOJ (Japan), STFC (U.K.), NASA, ESA, and NSC (Norway).

References

Abramenko, V. I., Carbone, V., Yurchyshyn, V., et al. 2011, ApJ, 743, 133
Alfvén, H. 1947, MNRAS, 107, 211
Batchelor, G. K. 1950, Quarterly Journal of the Royal Meteorological Society, 76, 133
Berger, T. E., Löfdahl, M. G., Shine, R. A., & Title, A. M. 1998, ApJ, 506, 439
Berrilli, F., Del Moro, D., Consolini, G., et al. 2004, Sol. Phys., 221, 33
Berrilli, F., del Moro, D., Giordano, S., Consolini, G., & Kosovichev, A. 2003, in ESA Special Publication, Vol. 535, Solar Variability as an Input to the Earth's Environment, ed. A. Wilson, 47–52
Biferale, L., Boffetta, G., Celani, A., et al. 2005, Physics of Fluids, 17, 115101
Bonet, J. A., Márquez, I., Sánchez Almeida, J., et al. 2010, ApJ, 723, L139
Cadavid, A. C., Lawrence, J. K., & Ruzmaikin, A. A. 1999, ApJ, 521, 844
Cadavid, A. C., Lawrence, J. K., Ruzmaikin, A. A., Walton, S. R., & Tarbell, T. 1998, ApJ, 509, 918
Centeno, R., Socas-Navarro, H., Lites, B., et al. 2007, ApJ, 666, L137
De Pontieu, B., McIntosh, S. W., Carlsson, M., et al. 2007, Science, 318, 1574
De Rosa, M. L. & Toomre, J. 2004, ApJ, 616, 1242
de Wijn, A. G., Stenflo, J. O., Solanki, S. K., & Tsuneta, S. 2009, Space Sci. Rev., 144, 275
Del Moro, D. 2004, A&A, 428, 1007
Del Moro, D., Berrilli, F., Duvall, Jr., T. L., & Kosovichev, A. G. 2004, Sol. Phys., 221, 23
Del Moro, D., Giordano, S., & Berrilli, F. 2007, A&A, 472, 599
Hagenaar, H. J., Schrijver, C. J., Title, A. M., & Shine, R. A. 1999, ApJ, 511, 932
Hart, A. B. 1956, MNRAS, 116, 38
Ishikawa, R. & Tsuneta, S. 2009, A&A, 495, 607
Klafter, J., Blumen, A., & Shlesinger, M. F. 1987, Physical Review A, 35, 3081
Kosugi, T., Matsuzaki, K., Sakao, T., et al. 2007, Sol. Phys., 243, 3
Lagg, A., Solanki, S. K., Riethmüller, T. L., et al. 2010, ApJ, 723, L164
Lawrence, J. K., Cadavid, A. C., Ruzmaikin, A., & Berger, T. E. 2001, Physical Review Letters, 86, 5894
Lawrence, J. K. & Schrijver, C. J. 1993, ApJ, 411, 402
Leighton, R. B. 1964, ApJ, 140, 1547
Lepreti, F., Carbone, V., Abramenko, V. I., et al. 2012, ApJ, 759, L17
Lites, B. W., Kubo, M., Socas-Navarro, H., et al. 2008, ApJ, 672, 1237
Liu, Y., Zhang, H., Ai, G., Wang, H., & Zirin, H. 1994, A&A, 283, 215
Manso Sainz, R., Martínez González, M. J., & Asensio Ramos, A. 2011, A&A, 531, L9
Martínez González, M. J. & Bellot Rubio, L. R. 2009, ApJ, 700, 1391
Martínez Pillet, V., Del Toro Iniesta, J. C., Álvarez-Herrero, A., et al. 2011, Sol. Phys., 268, 57
Mosher, J. M. 1977, PhD thesis, California Institute of Technology, Pasadena.
Muller, R., Auffret, H., Roudier, T., et al. 1992, Nature, 356, 322
November, L. J. 1980, PhD thesis, Colorado Univ., Boulder.
November, L. J., Toomre, J., Gebbie, K. B., & Simon, G. W. 1981, ApJ, 245, L123
November, L. J., Toomre, J., Gebbie, K. B., & Simon, G. W. 1982, ApJ, 258, 846
Parker, E. N. 1972, ApJ, 174, 499
Parker, E. N. 1983, ApJ, 264, 642
Parker, E. N. 1988, ApJ, 330, 474
Parker, E. N. 1994, Spontaneous current sheets in magnetic fields : with applications to stellar x-rays. International Series in Astronomy and Astrophysics, Vol. 1. New York : Oxford University Press, 1994., 1
Petrovay, K. 2001, Space Sci. Rev., 95, 9
Pietarila Graham, J., Cameron, R., & Schüssler, M. 2010, ApJ, 714, 1606
Priest, E. R., Heyvaerts, J. F., & Title, A. M. 2002, ApJ, 576, 533
Rast, M. P. & Pinton, J.-F. m. c. 2011, Phys. Rev. Lett., 107, 214501
Richardson, L. F. 1926, Proceedings of the Royal Society of London. Series A, 110
Roudier, T., Lignières, F., Rieutord, M., Brandt, P. N., & Malherbe, J. M. 2003, A&A, 409, 299
Roudier, T., Malherbe, J. M., Vigneau, J., & Pfeiffer, B. 1998, A&A, 330, 1136
Roudier, T. & Muller, R. 2004, A&A, 419, 757
Schrijver, C. J. & Martin, S. F. 1990, Sol. Phys., 129, 95
Shine, R. A., Simon, G. W., & Hurlburt, N. E. 2000, Sol. Phys., 193, 313
Simon, G. W. & Leighton, R. B. 1964, ApJ, 140, 1120
Simon, G. W., Title, A. M., & Weiss, N. O. 1995, ApJ, 442, 886
Stein, R. F. & Nordlund, A. 1989, ApJ, 342, L95
Thornton, L. M. & Parnell, C. E. 2011, Sol. Phys., 269, 13
Tomczyk, S., McIntosh, S. W., Keil, S. L., et al. 2007, Science, 317, 1192
Tsuneta, S., Ichimoto, K., Katsukawa, Y., et al. 2008, Sol. Phys., 249, 167
van Ballegooijen, A. A., Asgari-Targhi, M., Cranmer, S. R., & DeLuca, E. E. 2011, ApJ, 736, 3
van Ballegooijen, A. A., Nisenson, P., Noyes, R. W., et al. 1998, ApJ, 509, 435
Wang, H. 1988, Sol. Phys., 116, 1
Zhang, J., Lin, G., Wang, J., Wang, H., & Zirin, H. 1998, Sol. Phys., 178, 245
Zhou, G. P., Wang, J. X., & Jin, C. L. 2010, Sol. Phys., 267, 63